



## Synergistic Potential of Metal Nanoparticles Infused with Activated Carbon: Unveiling Antimicrobial and Photocatalytic Powers

F. Sowmiya<sup>1</sup> and S.R. Brintha<sup>2\*</sup>

<sup>1</sup>Research Scholar, Department of Chemistry, Annai Velankanni College, Tholayavattam, Kanyakumari, 629157, Manonmaniam Sundaranar University, Tirunelveli, 627012.

<sup>2</sup>Associate professor, Department of Chemistry, Annai Velankanni College, Tholayavattam, Kanyakumari, 629157, Manonmaniam Sundaranar University, Tirunelveli, 627012.

\*Corresponding Author: S.R. Brintha

\*Associate professor, Department of Chemistry, Annai Velankanni College, Tholayavattam, Kanyakumari, 629157, Manonmaniam Sundaranar University, Tirunelveli, 627012.

### KEYWORDS

Mukia maderaspatana, UV visible spectroscopy, X-ray Diffraction, Fourier Transform Infrared spectroscopy, Scanning electron microscopy, photocatalytic activity

### ABSTRACT:

Plants used for medical purposes have always had a significant impact in a variety of contexts across the globe. A kind of plant known as *Mukia maderaspatana* can only be found in environments that are warm and humid year-round. It is well-known for the medicinal virtues that it has and has been used for this purpose since ancient times. In the present investigation, the selected plant served as the raw material for the production of activated carbon. In addition to that, the plant was used to integrate nanoparticles of metals like cerium and manganese into the material. In the field of biological research, characterization methods such as UltraViolet visible spectroscopy (UV-Vis), X-ray diffraction analysis (XRD), Fourier transform infrared spectroscopy (FTIR), and scanning electron microscopy (SEM) are often used. The metal nanoparticles and activated carbon-doped metal nanoparticles were tested for their ability to inhibit the growth of *Bacillus subtilis*, *Staphylococcus aureus*, *Escherichia coli*, *Klebsiella pneumoniae*, *Aspergillus niger*, and *Aspergillus flavus*. The results showed that both types of nanoparticles have antibacterial and antifungal properties. The photocatalytic activity of the nanoparticles was studied, and the results showed a promising degrading activity at varied concentrations of nanoparticles over a certain amount of time.

### Introduction

Plants are necessary for our existence since they provide us with food and many medicines. Ayurveda, siddha, unani, and naturopathy represent some of the different types of traditional medical practices that are practiced in India. These medical procedures relied on different kinds of plants and were developed by different ancestral ethnic groups. It has been found that using certain plants' edible portions to cure certain illnesses can be beneficial. *Mukia maderaspatanus*, scientifically referred to as *Cucumis maderaspatanus*, is a botanical species characterised by its climbing habit. This particular species exhibits a wide distribution range, spanning across various tropical and subtropical regions. The presence of amino acids and alkaloids within the plant is believed to be associated with the causation of parasitic infection in cattle. Phytochemistry on *M. maderaspatana* uncovered the existence of several phytochemicals. Because of the abundance of hydroxyl groups in these phytochemical compounds found in *M. maderaspatana*, it boosts the antioxidant activity of these compounds, they are powerful reducing

agents (Priya et al., 2012). It possesses a wide variety of pharmacological effects, including antibacterial activity, antioxidant activity, anti-inflammatory activity, anti-diabetic activity, anti-cancer activity, anti-mitotic activity, gastroprotective action, anti-wart activity, anti-larvicidal activity, and anti-helminthic activity, and several others (Kumar et al., 2022).

In the same way that other medicinal plants have been employed in the production of activated carbon, *Mukia maderaspatana* is being used in the research that is now being conducted. Activated carbon, a kind of carbon that has the capabilities of being able to absorb substances due to its large surface area. The production of it involves heating carbon-rich materials like as wood, peat, coconut shells, or sawdust in the presence of a gas that does not react with the substance, leaving behind a porous structure in its wake. The seeds and shells of *Inga feuillei* and *Passiflora ligularis*, as well as the wood of *Kageneckia lanceolata*, *Baccharis salicifolia*, and *Baccharis latifolia*, have been the subject of studies pertaining to the production of activated carbon (Montalvo Andia et al., 2020).



In antimicrobial research, an innovative technique that involves the embedding of metallic nanoparticles on activated carbon has been created and has shown promising results. In the treatment of microorganisms, activated carbon derived from natural sources has been investigated as a potential effective adsorbent in recent times. Due to the huge specific surface area and porous character of activated carbon, it has a larger affinity for adsorbing organic compounds at lower concentrations. This is because to the carbon's porous structure. It has been determined that metallic nanoparticles impregnated with activated carbon, which is an effective nanomaterial for inhibiting the growth of microorganisms (Srinivasan et al., 2013).

The antibacterial activity of activated carbon doped metal nanoparticles synthesised from *Mukia maderaspatana* was examined earlier using both positive and negative bacterial strains, such as *Staphylococcus aureus*, *Staphylococcus epidermidis*, *Pseudomonas aeruginosa*, and *Escherichia coli*, in addition to one fungal strain, *Candida albicans*. The findings demonstrated that the nanoparticles were successful in combating a wide variety of bacterial and fungal pathogens. (Saravanan et al., 2016).

Under the influence of light, photodegradation activity by metal nanoparticles includes the use of metal nanoparticles as catalysts in photocatalytic processes to break down or degrade organic contaminants. This process is known as photodegradation activity. The science associated with photodegradation, which makes use of nanoparticles of metal, is always developing, and there is always research going on that aims to improve the effectiveness, selectivity, and practical application of these photocatalytic systems. Subsequently, experiments were conducted to examine the photodegradation of methylene blue using UV and sunlight exposure, aiming to assess the photocatalytic efficiency of the nanoparticles. (Shahmoradi et al., 2012).

#### Materials and Methods Synthesis of activated carbon doped metal nanoparticles

To eliminate debris, the leaves were rinsed with tap water. Five days later, it was desiccated in the shade after being sliced into small segments measuring 0.5 cm. The specimens underwent multiple washes with distilled water before being desiccated overnight at 110°C in an oven. For experimental purposes, the desiccated sample was subsequently enclosed in the container. A dehydrating agent consisting of 10 mL of phosphoric acid ( $H_3PO_4$ ) is utilized to impregnate the desiccated sample. The Erlenmeyer flask containing the sample (5g) was submerged in water and agitated with an  $H_3PO_4$  solution in a water bath shaker for three days at 80 °C and 70 rpm. Soaking and shaking the sample guarantees that the reagent is completely absorbed by the raw material. The samples were desiccated at 110 °C for 24 hours following the transfer into a Petri dish following

the impregnation process. They were subsequently transferred to a sterile crucible, weighed, covered with a lid, and stored in an airtight container pending further processing. A furnace utilized in the semi-carbonization and activation processes. Prior to placing the samples into the furnace, the furnace's temperature was maintained at 200°C. The sample was subsequently semi-carbonized for 15 minutes before the temperature of the furnace was adjusted to 500°C, the desired activation temperature, and the sample was activated for an additional 45 minutes. The chemical AC was subsequently reconstituted with distilled water for a duration of three hours. This process was iterated multiple times until a consistent pH was achieved. In the context of physical activation, 0.1 M  $HNO_3$  was utilized to flush AC in order to eliminate heavy metal ions, creosote, and ash. It was then repeatedly flushed with distilled water in the second phase in order to eliminate the acid. The AC was dry at 105°C for four hours in an oven (Anisuzzaman et al., 2015).

#### Encapsulation of Nanoparticles on Activated Carbon Granules

5-gram sample of treated activated carbon granules was immersed in a 200 ml solution containing manganese oxide (MnO) and cerium (Ce) nanoparticles with a concentration of 0.05 gms. The mixture was vigorously stirred at room temperature overnight to ensure that the coating process was fully done. The activated carbon, along with MnO and Ce nanoparticles, underwent a curing process in a vacuum oven at a temperature of 110°C for a minimum of 2 hours. This allowed for complete coating of the nano-particles onto the activated carbon. Therefore, manganese (II) acetate (MnOAC) and cerium(III) acetate (CeAC) were synthesized. The verification of the preparation was conducted by assessing the change in mass of the activated carbon granules prior to and following the coating procedure. (Abdel Hameed et al., 2013).

#### Characterization of metal nanoparticles and activated doped metal nanoparticles

The techniques of UV Visible spectrophotometry, X-ray diffraction analysis, Fourier transform infrared spectroscopy (FTIR), and scanning electron microscopy (SEM) were used in the research on the size and shape of metal nanoparticles, as well as activated carbon doped Cerium and Manganese nanoparticles.

#### Anti-microbial activity

The test microorganisms used for antibacterial analysis, bacteria *Escherichia coli*, *Klebsiella pneumonia*, *Bacillus subtilis*, *Staphylococcus aureus* and *Pseudomonas aeruginosa* and fungi *Aspergillus niger*, *Aspergillus flavus* and *Candida albicans* were purchased from Microbial Type Culture Collection and Gene Bank (MTCC) Chandigarh. The bacterial strains were maintained on Nutrient Agar (NA). The purified



culture obtained from the plate was inoculated onto a Nutrient Agar plate and subsequently sub cultured at a temperature of 37°C for a duration of 24 hours. The inoculum was created by aseptically introducing the newly grown culture into a 2 ml tube of sterile 0.145 mol/L saline solution. The cell density was then modified to match the 0.5 McFarland turbidity standard, resulting in a bacterial suspension with a concentration of  $1.5 \times 10^8$  cfu/ml.

The medium was created by solubilizing 38 grams of Mueller-Hinton Agar Medium in 1000 ml of distilled water. The aqueous solution was sterilized using autoclaving under a pressure of 15 lbs at a temperature of 121°C for a duration of 15 minutes, while maintaining a pH of 7.3.

The sterilized nutrient solution was cooled, thoroughly mixed, and transferred onto petri plates (25 ml per plate). The plates were inoculated with pathogenic bacterial cultures, including *Escherichia coli*, *Klebsiella pneumoniae*, *Bacillus subtilis*, *Staphylococcus aureus*, and *Pseudomonas aeruginosa*. The standard drug Linezolid 30 mcg and Ciprofloxacin 5 mcg concentration disc were employed as positive controls, depending on the sensitivity of the bacterial culture. An empty sterile disc was used as the negative control. The petri dishes were placed in an incubator set at a temperature of 37°C for a duration of 24 hours.

Following the completion of incubation, the presence of inhibition zones surrounding the disc was observed and quantified using a transparent ruler, with measurements recorded in millimeters. The diameter of the zone of inhibition was measured in millimeters. The lack of zone inhibition was interpreted as the lack of biological activity (Kohner *et al.*, 1994; Mathabe *et al.*, 2006; Assam *et al.*, 2010)

Antibiotic susceptibility tests were determined by agar disc diffusion (Kirby-Bauer) method. Fungal strains *Aspergillus niger*, *Aspergillus flavus* and *Candida albicans* were swabbed using sterile cotton swabs on SDA agar plate. Up to 80 µl of 1 mg/ml concentration of the extract was introduced in the sterile discs (10 mm) using sterile pipettes. The standard drug Fluconazole 150 mcg concentration was introduced in the sterile disc (10 mm) for positive control and empty sterile disc was used for negative control.

The disc was subsequently positioned on the surface of SDA medium, enabling the compound to undergo diffusion for a duration of 5 minutes. Following this, the plates were incubated at a temperature of 22°C for a period of 48 hours. Following the completion of incubation, the presence of inhibition zones surrounding

the disc was observed and quantified using a transparent ruler, with measurements recorded in millimeters.

#### Photo catalytic activity

The photo catalytic degradation efficiency of Cerium Nanoparticles (CeNps) and Manganese Nanoparticles (MnNps) were studied by varying irradiation time using batch mode experiments.

The photocatalytic activity of CeNps and MnNps, were explored for the degradation of methylene blue dye in the presence of sun light and also varied irradiation time. In this process, each nano particle samples (0.1 g) were added into separate conical flask containing 100 ml solution of methyleneblue dye (10 mg/l) at stable temperature. The catalyst and dye solution were being agitated on a magnetic stirrer in a dark environment to achieve equilibrium. Following the establishment of equilibrium, dye solutions were subjected to solar irradiation to induce photo degradation. 5 mL of biological sample was collected at different time points and subjected to centrifugation to separate the cellular components. The measurement of light absorption by the extracted solutions was recorded using a UV-visible spectrophotometer at a wavelength of 664 nm.

The percentage photo degradation of dyes was calculated using the formula as

$$\% \text{ Degradation} = \frac{A_0 - A}{A_0} \times 100$$

$A_0$  = Initial absorbance of dye

A = Absorbance of dye solution after solar irradiation

#### Results and Discussion

##### UV -Visible Spectroscopy

The use of UV-Vis spectroscopy is often mentioned as being one of the most feasible ways for the characterization of nanoparticles. Through the use of UV-vis spectroscopy, researchers were able to determine that the MnNPs exhibited the highest level of absorption at a wavelength of 258 nm, which corresponds to the absorption maximum of Mn nanoparticles. The appearance of an absorption edge at a wavelength of 258 nm may provide irrefutable evidence that manganese nanoparticles were created during the experiment. The reference range is similar to that of the earlier articles, which demonstrated a maximum peak however, the reference range for UV visible spectrophotometry falls somewhere between 200 and 800 nm (Souri *et al.*, 2018).

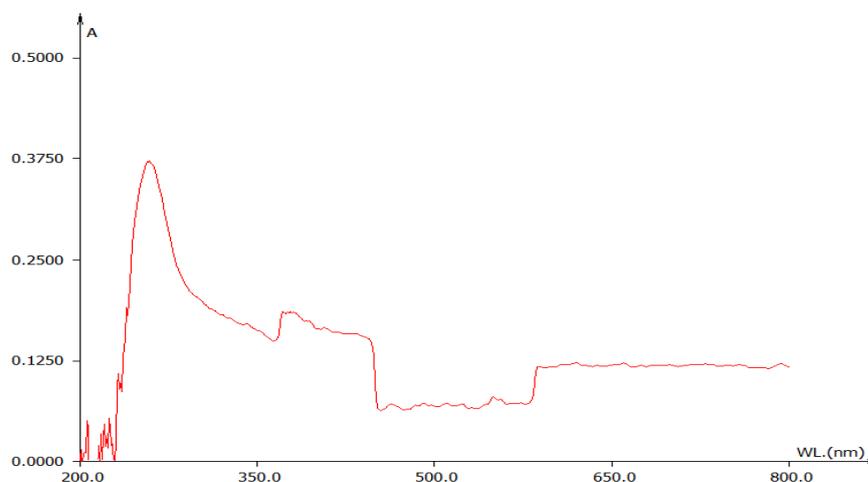


**Fig:** UV vis spectroscopy of Mn Nanoparticles

The ultraviolet-visible (UV-Vis) spectroscopy analysis revealed that the cerium nanoparticles exhibited a maximum absorption spectrum at a wavelength of 219 nm. The UV-visible spectra obtained in another demonstrated that the CeO<sub>2</sub> particles that were synthesized have a nanosized homogeneous size

distribution and absorb UV light in the region of 250-400 nm (Gu et al., 2007). There are findings that shows the presence of distinct absorption bands seen at 317, 280, 318, and 306 nm in the four separate samples of cerium nanoparticles (Goharshadi et al., 2011).

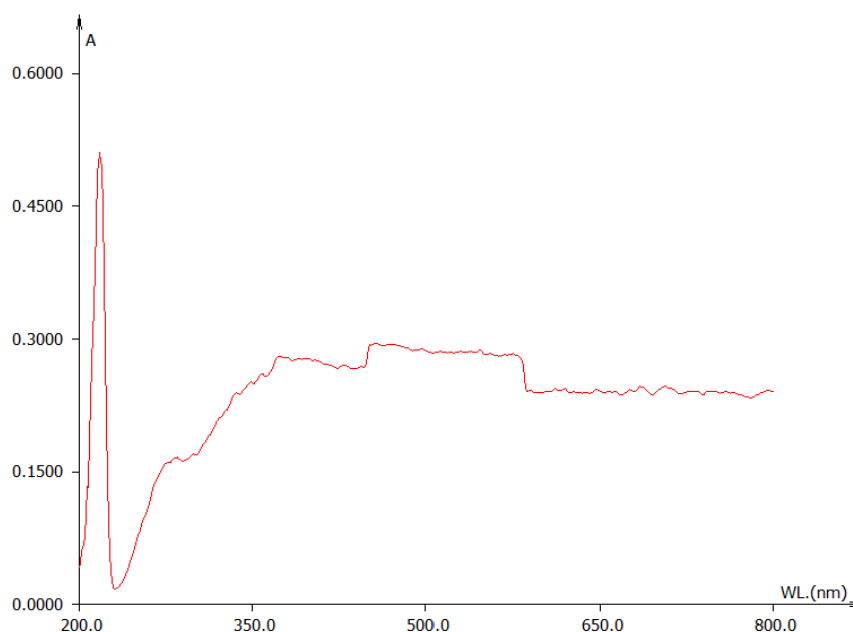


**Fig:** UV visible spectroscopy of Ce Nanoparticles

#### **XRD**

The values of 7.983°, 9.338°, 16.148°, 21.280°, 32.730°, and 58.380° were found to be present in the diffraction peaks that were seen in the manganese nanoparticles. However, these peaks do not exhibit a robust and distinct

character like the strong peaks seen in prior research on manganese nanoparticles that revealed peaks at 34.702°, 35.12°, and 32.27°. These strong peaks were detected in the previous studies on manganese nanoparticles.

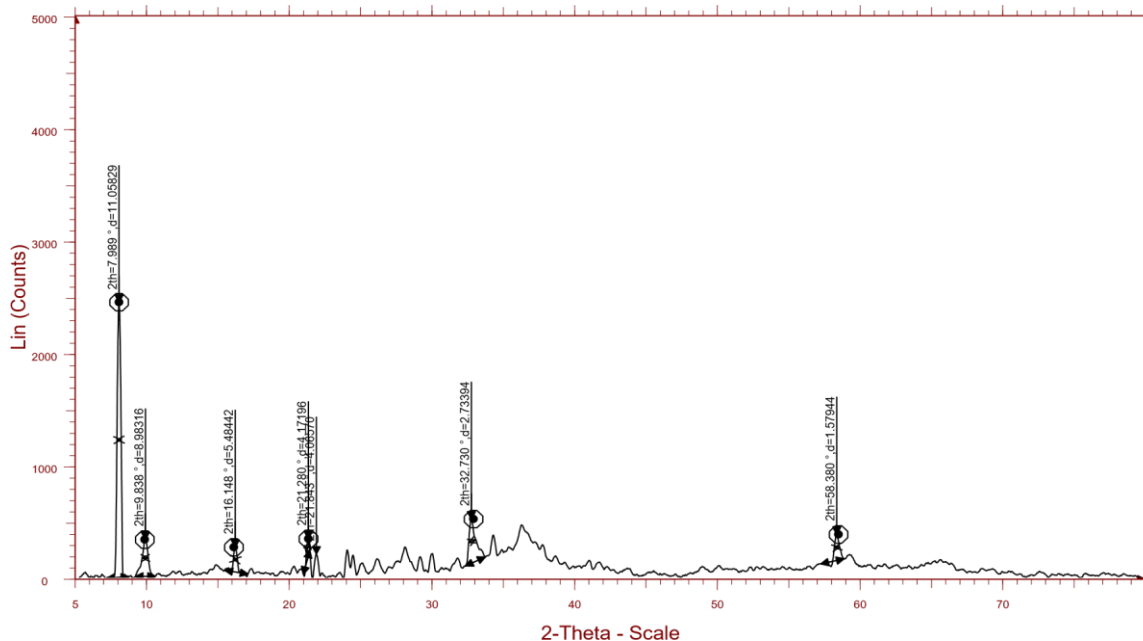
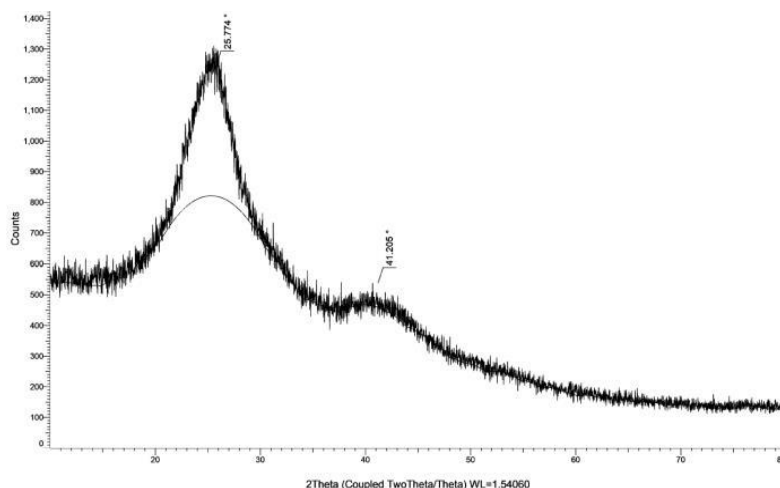


Fig: XRD analysis of Manganese nanoparticles

XRD analysis was performed to investigate the crystalline phase of activated carbon manganese nanoparticles and their composite, as well as to check for any defects in the material. It was observed that the diffraction peaks were located at 25.774° and 41.205°. A comparable investigation demonstrated that the X-ray diffraction pattern within the angle range of 10°C-80°C

of the manganese nanoparticles composite exhibited peaks at 28.33°, 40.53°, and 50.01° at 2θ. These peaks correspond to the face-centered cubic structure of manganese and align closely with the JCPDS No. 04-0326 reference (Kamran et al., 2018).



The XRD patterns of Ac-Ce nanoparticles displayed diffraction peaks at 18.909°, 27.419°, 28.951°, 40.524°, 56.239°, and 59.927°. These results were compared to the XRD patterns of Cerium nanoparticles, which were 28.089° and 48.041°. In contrast with the JCPDS file (PCPDF 34-0394) found in the database, all of the peaks

on the patterns are in remarkable cohesion, and the diffraction peaks revealed cubic structure. The results of this were compared to those of earlier investigations that demonstrated diffraction peaks of a similar kind (Jayakumar et al., 2019 and Lin et al., 2003).

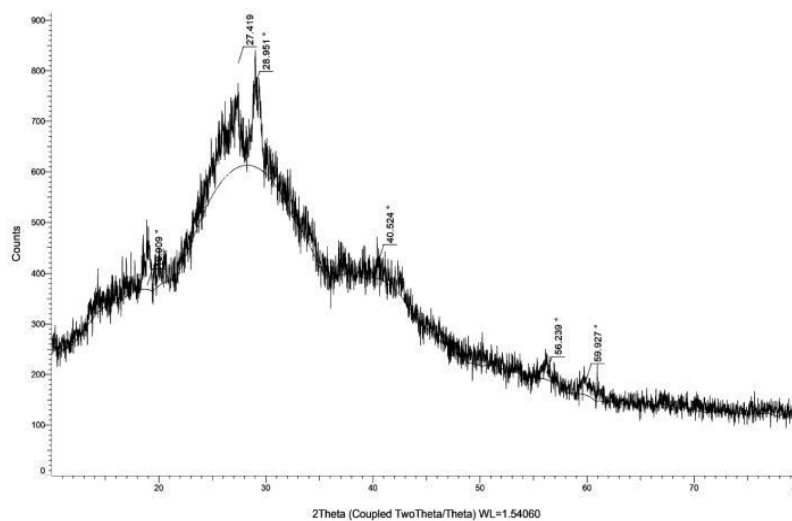


**Fig:** XRD of Activated carbon doped cerium nanoparticles

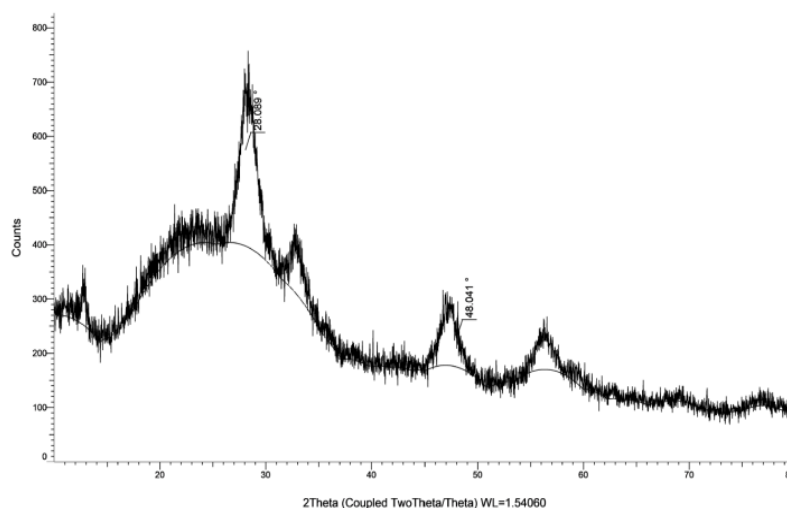


**Fig:** XRD of cerium nanoparticles

### FTIR

The spectral features observed within the range of 400 to 4000  $\text{cm}^{-1}$  corresponded to distinct peaks located at 3218, 2988, 1936, 1636, and 1070  $\text{cm}^{-1}$ . Among these, the band 1070 exhibits a distinct peak and corresponds to the stretching of C-O bonds, while the remaining bands display a moderate intensity. 3218  $\text{cm}^{-1}$  corresponds to the stretching of hydroxyl (OH) groups, 2988  $\text{cm}^{-1}$  resembles the stretching of carbon-hydrogen (C-H) bonds, vibration at 1936  $\text{cm}^{-1}$  matches with the

stretching of carbon-carbon-carbon (C=C=C) bonds, and  $\text{cm}^{-1}$  corresponds to the bonding of carbon-carbon (C=C) double bonds. This observation exhibited a correlation with the investigations performed on Mn Nanoparticles, which demonstrated the presence of a band at 1643  $\text{cm}^{-1}$ , indicative of C-O stretching (He et al., 2021). In the case of the MnO<sub>2</sub> nanoparticles, it was seen that medium bands coexisted with the sharp band at 1236  $\text{cm}^{-1}$  and below 1000  $\text{cm}^{-1}$  (Jaganyi et al., 2013).

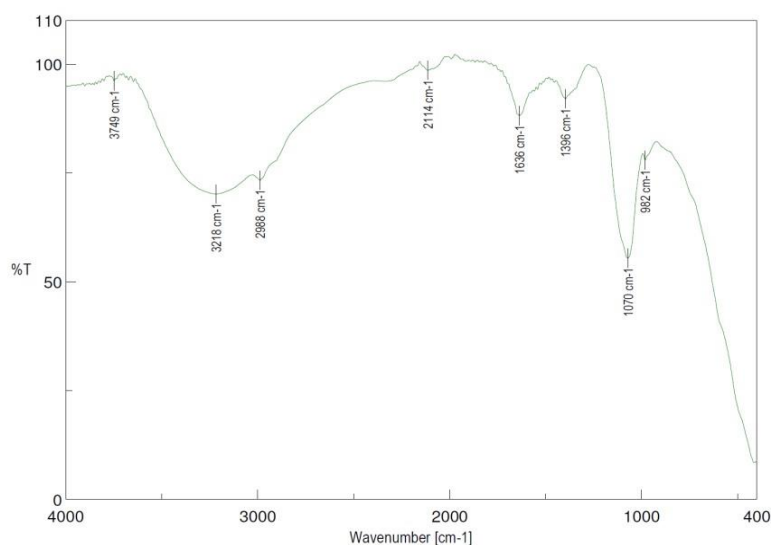


**Fig:** FTIR of manganese nanoparticles

The spectral peaks observed for the activated carbon doped Manganese nanoparticle are located at wavelengths of 3815, 3745, 3606, 3163, 2334, 1558, 1164, 884, 806, 784, 739, 676, 646, and 620  $\text{cm}^{-1}$ . Among these, the peaks at 1558  $\text{cm}^{-1}$  and 1164  $\text{cm}^{-1}$  are distinct and represent the stretching vibrations of N-O

and C-O bonds, respectively. These bands exhibit similarities to the bands observed in previous studies involving Activated carbon doped Manganese nanoparticles (Khan et al., 2019).

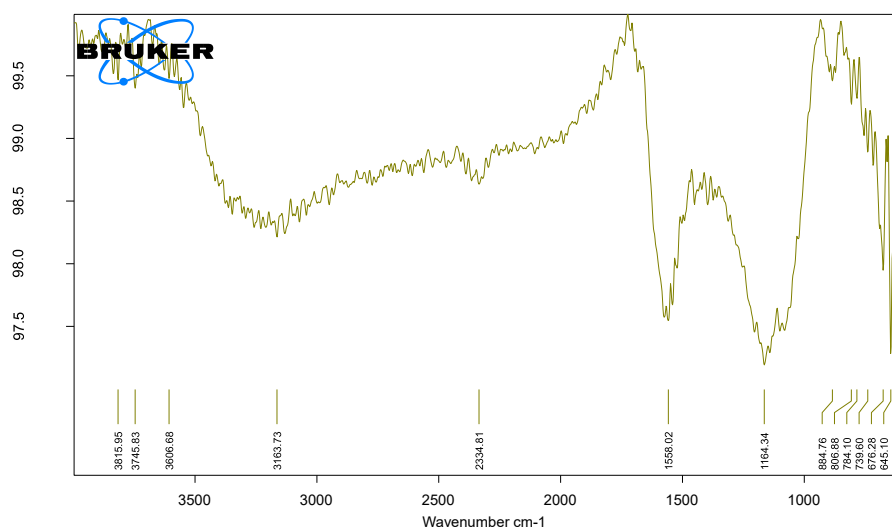


**Fig:** FTIR of activated carbon doped manganese nanoparticle

The spectral peaks of the cerium nanoparticle may be seen at the following wavelengths: 3349, 2985, 1725, 1660, 150, 1482, 1380, 1049, 830, and 688  $\text{cm}^{-1}$  correspondingly. Band 3349  $\text{cm}^{-1}$  is wide and indicates the O-H stretching; weak bands 2985  $\text{cm}^{-1}$  and 1725  $\text{cm}^{-1}$  reflect the existence of O-H bending and C-H bending; medium bands 1660  $\text{cm}^{-1}$  and 1550  $\text{cm}^{-1}$  reflect C=C and NO stretching. Sharp bands may be seen at 1380  $\text{cm}^{-1}$

and 1049  $\text{cm}^{-1}$ , which is evidence of S=O and C-F bending. The bending of C=C and stretching of C-Br may be seen in the bands at 830  $\text{cm}^{-1}$  and 688  $\text{cm}^{-1}$ . These bands contain features that are similar to those of bands discovered in prior studies employing cerium nanoparticles that had the earlier bands had maxima at 3465, 2495, 2397, 1464, 1298, 1036, and 741  $\text{cm}^{-1}$  respectively (Farahmandjou et al., 2016).

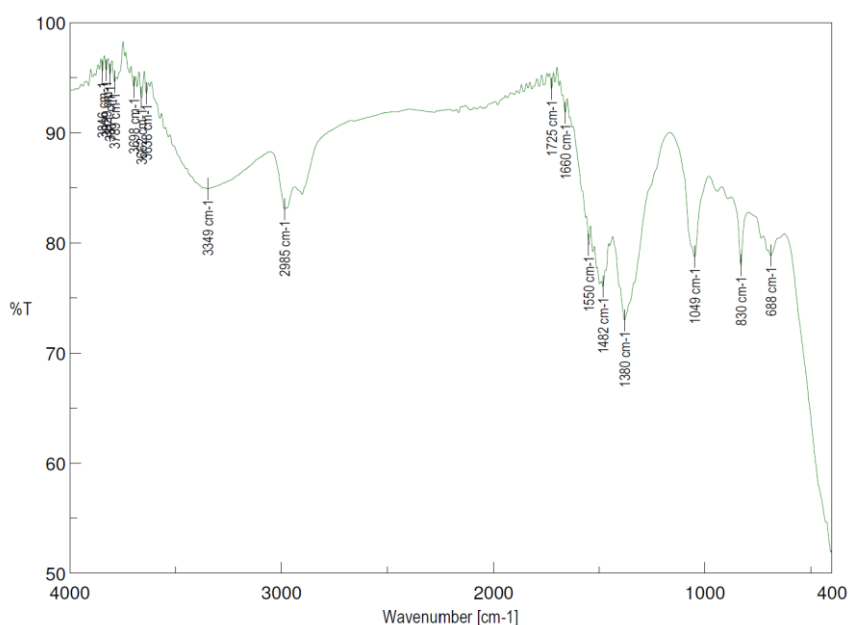


**Fig:** FTIR of cerium nanoparticles

The activated carbon doped cerium nanoparticle has spectral peaks that are seen at wavenumbers of 3848, 2360, 1570, 1053, 885, 836, 817, 786, 744, 717, 685, 653, and 627  $\text{cm}^{-1}$  respectively. The band 1053  $\text{cm}^{-1}$  is the only one of them that is both sharp and strong, which indicates that it is bending CO more strongly than the other bands. The bands below 700  $\text{cm}^{-1}$  also feature several short and sharp bands that show strong and

medium C=C bending. The C-H and C=C stretching patterns are matched by the medium bands at 3848  $\text{cm}^{-1}$  and 1570  $\text{cm}^{-1}$ . These bands have characteristics that are comparable to those of bands found in earlier research utilizing activated carbon doped cerium nanoparticles, which included maxima at 1640, 3400, 2900, and 1054  $\text{cm}^{-1}$ , as well as a sharp band at 500  $\text{cm}^{-1}$  (Alhooshani et al., 2015).

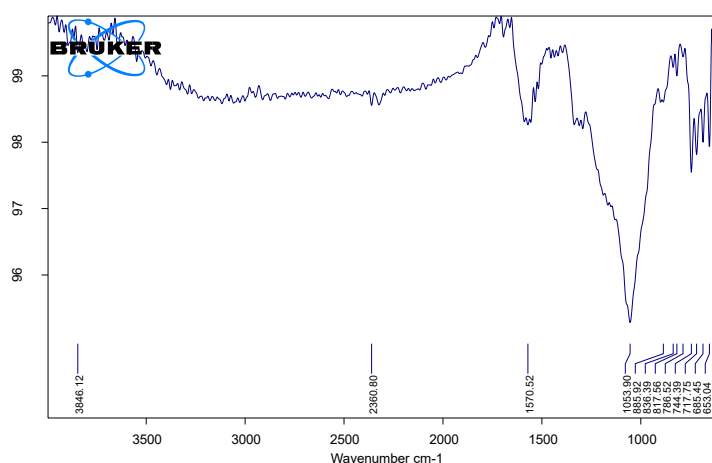


**Fig:** FTIR of activated carbon doped cerium nanoparticles

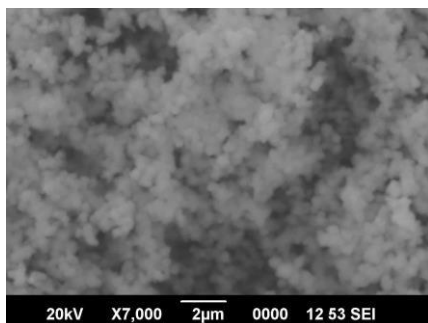
### SEM

According to the analysis of the SEM micrograph, the particle size of the Mn nanoparticles is 30 nm. A prior study demonstrated that the scanning electron microscopy (SEM) pictures of manganese oxide nanoparticles exhibited the presence of mostly spherical particles that were agglomerated. The grain size was determined to be 12 nm using SEM (Vijayamari et al.,

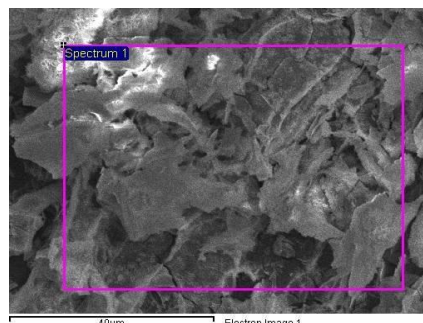
2016). According to the findings of yet another research, the size of manganese nanoparticles based on the SEM analysis and other characterisation analysis, the size is less than 100 nm (Khan et al., 2019).

The scanning electron micrograph showed that the CeO<sub>2</sub> nanoparticles that had been generated with a big size had a shape similar to a sphere and had an average particle size of 110 nm (Jayakumar et al., 2017). This is

consistent with the investigations that are now being carried out, which have shown that the size of cerium nanoparticles is 90 nm.



SEM image of Mn nanoparticle



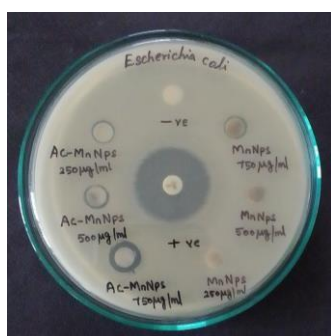
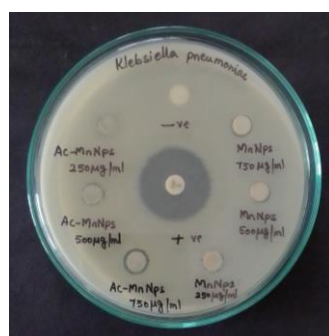
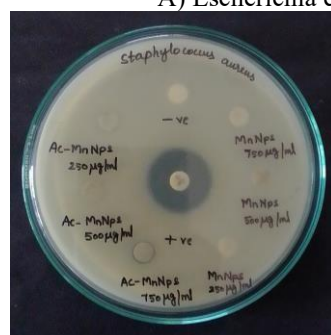
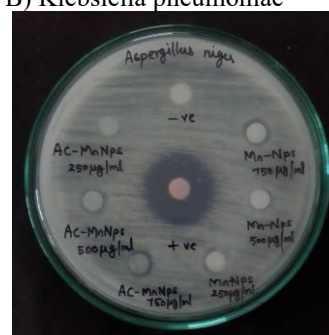
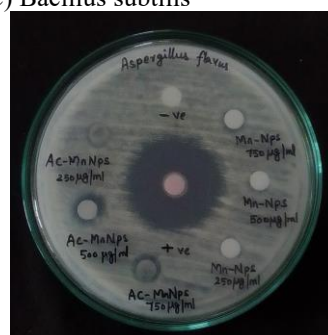
SEM image of Ce nanoparticle

Fig: Images of Mn and Ce nanoparticles

### Antimicrobial activity

The antimicrobial efficacy of manganese nanoparticles was observed, revealing a zone of inhibition measuring 7mm against both *E. coli* and *Bacillus subtilis* when exposed to a concentration of 750 µg/ml. However, no zone of inhibition was observed at lower concentrations. *Klebsiella pneumoniae* exhibited a notable inhibition zone measuring 7 mm when exposed to concentrations of 250 and 500 µg/ml. Furthermore, at higher concentrations, the inhibition zone expanded to 8 mm. No zones of inhibition were observed in the presence of *Staphylococcus aureus*. The observed phenomenon involved the utilisation of activated carbon doped manganese nanoparticles, which exhibited varying

degrees of inhibitory effects against *Escherichia coli*. The respective concentrations of these nanoparticles resulted in zone of inhibition measurements of 7, 8, and 11 mm, indicating a progressive increase in the inhibitory potential. There was observed an inhibition of 7, 8, and 9 mm against the bacterium *Klebsiella pneumoniae*. In *Bacillus subtilis*, a decrease in concentration resulted in the observation of an 8 mm zone of inhibition, while at higher concentrations, 9 mm zone of inhibition was observed. A zone of inhibition measuring 7 mm was observed when exposed to a concentration of 750 µg/ml against *Staphylococcus aureus*. However, no zone of inhibition was observed at lower concentrations.

A) *Escherichia coli*B) *Klebsiella pneumoniae*C) *Bacillus subtilis*D) *Staphylococcus aureus*E) *Aspergillus niger*F) *Aspergillus flavus*Fig : Images of zones formed in A) *Escherichia coli*, B) *Klebsiella pneumoniae* C)



**Bacillus subtilis, D) Staphylococcus aureus, E) Aspergillus niger and F) Aspergillus flavus by Manganese nanoparticles and Activated carbon doped Manganese nanoparticles** Manganese nanoparticles exhibited notable antifungal properties, as evidenced by the formation of a discernible zone of inhibition measuring approximately 7mm at concentrations of 250 and 500 mg, and 8mm at a concentration of 750 mg. Equivalent sizes of regions were observed in both fungal specimens when exposed

to a concentration of 250 mg of activated carbon-doped manganese nanoparticles (MnNPs). The antimicrobial activity exhibited a moderate response, as evidenced by the relatively greater zone sizes observed in the positive control compared to the zones formed by the nanoparticles and activated carbon doped metal nanoparticles. This observation provides a comprehensive understanding of the antimicrobial properties under investigation.

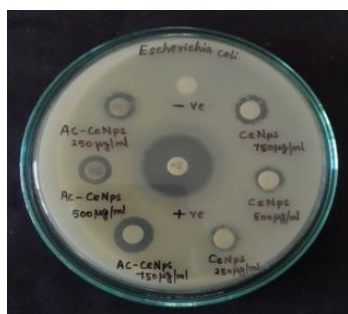
**Table:** zone of inhibition formed by Manganese nanoparticles and activated carbon doped Manganese nanoparticles against bacteria and fungi

Bacteria	Zone of inhibition (mm)						Positive control	Negative control
	MnNPs			AcMnNPs				
	250 µg/ml	500 µg/ml	750 µg/ml	250 µg/ml	500 µg/ml	750 µg/ml		
<i>Escherichia coli</i>	NZ	NZ	7 mm	7 mm	8 mm	11mm	23 mm	NZ
<i>Klebsiella pneumoniae</i>	7 mm	7 mm	8 mm	7 mm	8 mm	9 mm	24 mm	NZ
<i>Bacillus subtilis</i>	NZ	NZ	7 mm	8 mm	8 mm	9 mm	24 mm	NZ
<i>Staphylococcus aureus</i>	NZ	NZ	NZ	NZ	NZ	7 mm	21 mm	NZ
<b>Fungi</b>								
<i>Aspergillus niger</i>	7 mm	7 mm	8 mm	7 mm	8 mm	9 mm	23 mm	NZ
<i>Aspergillus flavus</i>	7 mm	7 mm	8 mm	7 mm	9 mm	10 mm	29 mm	NZ

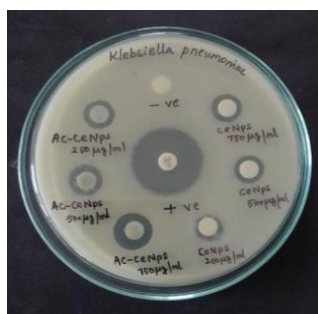
Cerium nanoparticles exhibit zone of inhibition measurements of 8mm, 9mm, and 11mm against *Escherichia coli*, while displaying zone of inhibition measurements of 8mm, 10mm, and 9mm against *Klebsiella pneumoniae*. *Bacillus subtilis* exhibits inhibitory activity of 7mm, 10mm, and 9mm, as well as a zone of inhibition measuring 7mm, 8mm, and 7mm against *Staphylococcus aureus*. In a similar vein, it has been observed that carbon-doped cerium nanoparticles exhibit reduced efficacy against pathogens when compared to their metallic nanoparticle counterparts. In *Klebsiella pneumoniae*, the presence of inhibition was observed at concentrations of 7 mm and 8 mm, denoting varying degrees of inhibitory effect. A measure of 7 mm of activity was observed against *Bacillus subtilis* and *E. coli* when exposed to 750 µg/ml of the substance.

Conversely, no zone of inhibition was observed in the case of *Staphylococcus aureus*.

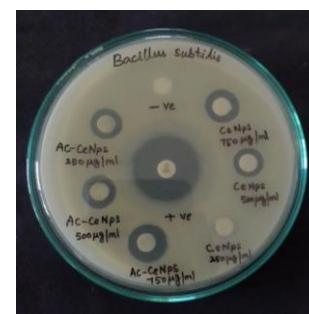
The CeNPs at concentrations of 250 and 500 mg demonstrated a zone of inhibition measuring 7 mm when tested against the fungal species *Aspergillus niger* and *Aspergillus flavus*. At a concentration of 750 mg, *Aspergillus niger* exhibited a 7mm zone of inhibition, which is comparatively smaller than the 8 mm zone of inhibition observed in *Aspergillus flavus*. Concurrently, the CeNPs doped with activated carbon demonstrated a 7 mm inhibition effect on the growth of *Aspergillus niger* and *Aspergillus flavus*. At a concentration of 750 mg, the observed inhibitory effect against *Aspergillus niger* was 7 mm, while against *Aspergillus flavus* it was 9 mm.



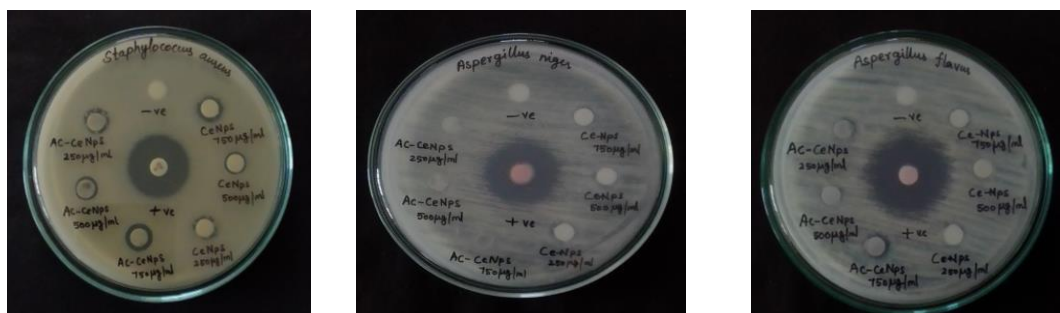
A) *Escherichia coli*



B) *Klebsiella pneumoniae*



C) *Bacillus subtilis*

D) *Staphylococcus aureus*E) *Aspergillus niger*F) *Aspergillus flavus*

**Fig :** Images of zones formed in A) *Escherichia coli*, B) *Klebsiella pneumoniae* C) *Bacillus subtilis*, D) *Staphylococcus aureus*, E) *Aspergillus niger* and F) *Aspergillus flavus* by cerium nanoparticles and Activated carbon doped Cerium nanoparticles

**Table:** zone of inhibition formed by Cerium nanoparticles and activated carbon doped Cerium nanoparticles against bacteria and fungi

Bacteria	Zone of inhibition (mm)							Positive control	Negative control
	CeNPs			AcCeNPs					
	250 µg/ml	500 µg/ml	750 µg/ml	250 µg/ml	500 µg/ml	750 µg/ml			
<i>Escherichia coli</i>	8 mm	9 mm	11mm	NZ	NZ	7 mm	23 mm	NZ	
<i>Klebsiella pneumoniae</i>	8 mm	10 mm	9 mm	7 mm	7 mm	8 mm	24 mm	NZ	
<i>Bacillus subtilis</i>	7 mm	10 mm	9 mm	NZ	NZ	7 mm	24 mm	NZ	
<i>Staphylococcus aureus</i>	7 mm	8 mm	7 mm	NZ	NZ	NZ	21 mm	NZ	
<b>Fungi</b>									
<i>Aspergillus niger</i>	7 mm	7 mm	7 mm	7 mm	7 mm	7 mm	23 mm	NZ	
<i>Aspergillus flavus</i>	7 mm	7 mm	8 mm	7 mm	7 mm	9 mm	25 mm	NZ	

### Photocatalytic activity

At the 10-minute mark, a quantity of 0.02 g of MnNPs experienced a degradation of 34.5%. This degradation rate subsequently increased to 38.86% at 20 minutes, 40.05% at 30 minutes, 51.64% at 40 minutes, and finally reached 60.33% and 63.23% at 50 and 60 minutes, respectively. In a comparable manner, the mass of 0.04 g of MnNPs exhibited a degradation percentage ranging from 39.4% to 73.92% over a time span of 10 minutes to 60 minutes. A total mass of 0.06 g of MnNPs exhibited degradation percentages of 57.2%, 62.03%, 62.43%, 69.23%, 77.62%, and 79.72% over a time span ranging from 10 minutes to one hour. A quantity of 0.08

g of MnNPs exhibited a degradation rate of 72.12% after a duration of 10 minutes. Subsequently, the degradation percentage increased by 67.38%, 69.93%, 78.02%, 83.81%, and 86.01% at successive 10-minute intervals. At a concentration of 0.1 g, the MnNPs exhibited degradation rates of 66.53%, 70.82%, 74%, 77.62%, 84.41%, and 87.81% over a time span ranging from 10 minutes to 1 hour. Zn-manganese nanoparticles served as photocatalysts and demonstrated greater activity, which may destroy up to 99% of the dye after four hours of exposure to UV light. This finding goes along with the findings that have been obtained thus far (Anjuchanu et al., 2018).

**Table:** photocatalytic activity of activated carbon doped Mn nanoparticles

Time interval	Percentage of inhibition (%)				
	Concentration of AC-MnNPs (g)				
	0.02	0.04	0.06	0.08	0.1
<b>Initial</b>	-	-	-	-	-
<b>10 minutes</b>	34.5%	39.4%	57.2%	72.12%	66.53%
<b>20 minutes</b>	38.86%	59.34%	62.03%	67.38%	70.82%
<b>30 minutes</b>	40.05%	59.94%	62.43%	69.93%	74%
<b>40 minutes</b>	51.64%	60.03%	69.23%	78.02%	77.62%
<b>50 minutes</b>	60.33%	68.43%	77.62%	83.81%	84.41%
<b>60 minutes</b>	63.23%	73.92%	79.72%	86.01%	87.81%

**Table:** photocatalytic activity of activated carbon doped Ce nanoparticles

Time interval	Percentage of inhibition (%)				
	Concentration of AC-CeNPs (g)				
	0.02	0.04	0.06	0.08	0.1
Initial	-	-	-	-	-
10 minutes	76.9%	62.6%	51.3%	61%	35.7%
20 minutes	85.2%	79.5%	60.9%	75.1%	60.1%
30 minutes	89.7%	84.8%	80.5%	88.9%	74.2%
40 minutes	92.1%	94.4%	97.5%	98.7%	94.3%
50 minutes	92.6%	95.8%	98.5%	99.1%	99.5%
60 minutes	94.4%	97.9%	99.1%	99.9%	99.9%

The degradation of 0.02 g of CeNps was 76.9% after 10 minutes, rising to 85.2% after 20 minutes, 89.9% after 30 minutes, 92.1% after 40 minutes, and 92.6% and 94.4% after 50 and 60 minutes. In a similar vein, 0.04g of CeNps degraded from 62.6% to 97.9% during the course of 10 to 60 minutes. 51.3%, 60.9%, 80.5%, 97.5%, 98.5%, and 99.1% of CeNps' degradation was seen in 0.06g over a 10-minute to one-hour period. After 10 minutes, 0.08g of CeNps showed 61% degradation, and every 10 minutes, that percentage increased to 75.1%, 88.9%, 98.7%, 99.1%, and 99.9%. CeNps demonstrated 35.7%, 60.1%, 74.2%, 94.3%, 99.5%, and 99.9% degradation from 10 minutes to 1 hour at a concentration of 1 g. In a study that was connected to the present research, it was shown that Ce/ZnO-based photocatalysts had improved photocatalytic activity. These photocatalysts had the capacity to destroy 94.06% of MO after being exposed to the light for 60 minutes (Rodwihok et al., 2020). According to the findings of another investigation, the rate of degradation for methyleneblue at a concentration of 20 mg/L was 90.6% after 125 minutes (Pouretedal and Kadkhodaie, 2010).

### Conclusion

In conclusion, the synthesis of activated carbon from the plant *Mukia maderaspatana* shows a multidimensional strategy with potential applications in antibacterial and photodegradation activities. This technique is linked with the integration of nanoparticles of manganese and cerium. Dopants, such as manganese and cerium nanoparticles, are being added to activated carbon in order to bring about a strategic improvement in the activated carbon's characteristics. These metal nanoparticles have the potential to drastically affect the surface chemistry, porosity, and reactivity of the material, hence enhancing the material's capacity to inhibit the growth of microorganisms and to degrade under the impact of light. This study not only makes a contribution to the area of sustainable materials but also opens up new paths for solving important concerns in public health and the protection of the natural environment.

### References

- 1) Priya G.S., Radhika R., Siddhuraju P. Antioxidant and antimicrobial activity of traditional indian leavesy vegetables: *Mukia maderaspatana* and *Solanum trilobatum*. *Int. J. Pharm. Pharm. Sci.* 2012; 4:513–521.
- 2) Vasantha S. Kumar, Navaith Ahmed, John K. Alphonso, Shobana Chandrasekar, Usharani Boopathy" A Review on Pharmacological Activities of *Mukia Maderaspatana*." *International Journal of Health Sciences*, no. III, 1 May. 2022, pp. 4449-4459
- 3) Jayakumar, G.; Irudayaraj, A. Albert; Raj, A. Dhayal (2019). *Investigation on the synthesis and photocatalytic activity of activated carbon–cerium oxide (AC–CeO<sub>2</sub>) nanocomposite*. *Applied Physics A*, 125(11), 742–. doi:10.1007/s00339-019-3044-4
- 4) Shioh Shyung Lin; Dong Jang Chang; Ching-Huei Wang; Chia Chrn Chen (2003). *Catalytic wet air oxidation of phenol by CeO<sub>2</sub> catalyst—effect of reaction conditions*. , 37(4), 0–800. doi:10.1016/s0043-1354(02)00422-0
- 5) Kamran, U., Bhatti, H. N., Iqbal, M., Jamil, S., & Zahid, M. (2018). Biogenic synthesis, characterization and investigation of photocatalytic and antimicrobial activity of manganese nanoparticles synthesized from *Cinnamomum verum* bark extract. *Journal of Molecular Structure*. doi: 10.1016/j.molstruc.2018.11.00
- 6) He, F., Cai, W., Lin, J., Yu, B., Owens, G., & Chen, Z. (2021). Reducing the impact of antibiotics in wastewaters: Increased removal of mitoxantrone from wastewater by biosynthesized manganese nanoparticles. *Journal of Cleaner Production*, 293, 126207. doi:10.1016/j.jclepro.2021.126207
- 7) Jaganyi, D., Altaf, M. & Wekesa, I. Synthesis and characterization of whisker-shaped MnO<sub>2</sub> nanostructure at room temperature. *Appl Nanosci* 3, 329–333 (2013). <https://doi.org/10.1007/s13204-012-0135-3>
- 8) Khan, I., Sadiq, M., Khan, I., & Saeed, K. (2019). Manganese dioxide nanoparticles/activated carbon composite as efficient UV and visible-light



- photocatalyst. *Environmental Science and Pollution Research*. doi:10.1007/s11356018-4055-y
- 9) Alhooshani, K. R. (2015). Adsorption of chlorinated organic compounds from water with cerium oxide-activated carbon composite. *Arabian Journal of Chemistry*. doi:10.1016/j.arabjc.2015.04.013
  - 10) M. Farahmandjou, M. Zarinkamar and T.P. Firoozabadi, Synthesis of Cerium Oxide (CeO<sub>2</sub>) nanoparticles using simple CO-precipitation method, *Revista Mexicana de Física* 62 (2016) 496–499
  - 11) Soury M, Hoseinpour V, Shakeri A, Ghaemi N. Optimisation of green synthesis of MnO nanoparticles via utilising response surface methodology. *IET Nanobiotechnol*. 2018 Sep;12(6):822-827. doi: 10.1049/iet-nbt.2017.0145. PMID: 30104457; PMCID: PMC8676278.
  - 12) Goharshadi, E. K., Samiee, S., & Nancarrow, P. (2011). Fabrication of cerium oxide nanoparticles: Characterization and optical properties. *Journal of Colloid and Interface science*, 356(2), 473–480. doi:10.1016/j.jcis.2011.01.063
  - 13) Khan, I., Sadiq, M., Khan, I., & Saeed, K. (2019). Manganese dioxide nanoparticles/activated carbon composite as efficient UV and visible-light photocatalyst. *Environmental Science and Pollution Research*. doi:10.1007/s11356018-4055-y
  - 14) Rodwihok C, Wongratanaphisan D, Tam TV, Choi WM, Hur SH, Chung JS. CeriumOxide-Nanoparticle-Decorated Zinc Oxide with Enhanced Photocatalytic Degradation of Methyl Orange. *Applied Sciences*. 2020; 10(5):1697. <https://doi.org/10.3390/app10051697>
  - 15) Pouretedal, H. R., & Kadkhodaie, A. (2010). Synthetic CeO<sub>2</sub> Nanoparticle Catalysis of Methylene Blue Photodegradation: Kinetics and Mechanism. *Chinese Journal of Catalysis*, 31(11-12), 1328–1334. doi:10.1016/s1872-2067(10)60121-0
  - 16) AnjuChanu, L., Joychandra Singh, W., Jugeshwar Singh, K., & Nomita Devi, K. (2018). Effect of operational parameters on the photocatalytic degradation of Methylene blue dye solution using Manganese doped ZnO nanoparticles. *Results in Physics*. doi:10.1016/j.rinp.2018.12.089
  - 17) Montalvo Andia, J., Larrea, A., Salcedo, J., Reyes, J., Lopez, L., & Yokoyama, L. (2020). Synthesis and characterization of chemically activated carbon from *Passiflora ligularis*, *Inga feuillei* and native plants of South America. *Journal of Environmental Chemical Engineering*, 103892. doi:10.1016/j.jece.2020.103892
  - 18) J. N.R. Srinivasan, P.A. Shankar, R. Bandyopadhyaya, Plasma treated activated carbon impregnated with silver nanoparticles for improved antibacterial effect in water disinfection, *Carbon* 57 (2013) 1e10
  - 19) Saravanan, A., Kumar, P. S., Karthiga Devi, G., & Arumugam, T. (2016). Synthesis and characterization of metallic nanoparticles impregnated onto activated carbon using leaf extract of *Mukia maderasapatna*: Evaluation of antimicrobial activities. *Microbial Pathogenesis*, 97, 198–203. doi:10.1016/j.micpath.2016.06.019
  - 20) Shahmoradi, B., Negahdary, M., & Maleki, A. (2012). Hydrothermal Synthesis of Surface-Modified, Manganese-Doped TiO<sub>2</sub> Nanoparticles for Photodegradation of Methylene Blue. *Environmental Engineering Science*, 29(11), 1032–1037. doi:10.1089/ees.2011.0519
  - 21) Esraa Kareem Jassem, Aseel Mustafa Abdul Majeed and Nibras Mossa Umran, The Effect of Temperature on Structural and optical properties of Manganese Oxide Nanoparticles, *J. Phys.* (2019) Conf. Ser. 1279 012004
  - 22) Gu, H., & Soucek, M. D. (2007). Preparation and Characterization of Monodisperse Cerium Oxide Nanoparticles in Hydrocarbon Solvents. *Chemistry of Materials*, 19(5), 1103–1110. doi:10.1021/cm061332r
  - 23) Vijayamari, A., Sadayandi, K., Sagadevan, S., & Singh, P. (2016). A study of optical, surface morphological and electrical properties of manganese oxide nanoparticles. *Journal of Materials Science: Materials in Electronics*, 28(3), 2739–2746. doi:10.1007/s10854-016-5853-y
  - 24) G Jayakumar, A Albert Irudayaraj, A Dhayal Raj. Particle Size Effect on the Properties of Cerium Oxide (CeO<sub>2</sub>) Nanoparticles Synthesized by Hydrothermal Method. *Mechanics, Materials Science & Engineering Journal*, 2017, 9 (1).